Common intermediate species from reducing and activation of CoMo-based catalyst revealed via multivariate augmented system applied to time-resolved in situ XAS data

Danilo Oliveira de Souza, Asma Tougerti, Valérie Briois, Christine Lancelot, Sylvain Cristol

Common Intermediate Species from Reducing and Activation of CoMo-based Catalyst Revealed Via Multivariate Augmented System Applied to Time-Resolved *in situ* XAS data

Danilo Oliveira de SOUZA[*†], *Asma TOUGERTI*[†], *Valérie BRIOIS*[‡], *Christine LANCELOT*[†], *Sylvain CRISTOL*[†]

† Univ. Lille, CNRS, Centrale Lille, ENSCL, Univ. Artois, UMR 8181 – UCCS – Unité de Catalyse et Chimie du Solide, F-59000 Lille, France

‡ Synchrotron SOLEIL, UR1-CNRS L'Orme des Merisiers, Saint-Aubin, BP 48, 91192, Gif-sur-Yvette Cedex, France

*Corresponding author's current adress and correspondence: Elettra Sincrotrone Trieste, Strada Statale 14 - km 163,5 in AREA Science Park. 34149 Basovizza, Trieste ITALY. Tel. +39 040 375 8604, e-mail : danilo.oliveiradesouza@elettra.eu

Keywords: Chemometric methods; Hydrodesulfurization; CoMo catalyst; Time-resolved XAS

ABSTRACT

Time-resolved spectroscopy has reached great importance in studies of chemical transformations, particularly in heterogeneous catalysis, where *in situ* or *operando* conditions

are suitable to correlate precursor transformation and/or genesis of active sites with catalytic efficiency. In this work we present advantages of using chemometric analysis to resolve multi-step chemical reactions in time-resolved XAS experiment. We followed complementary experiments (temperature programmed reduction and activation) of a Ti-supported CoMo HDS catalyst to unravel details in the evolution of the different species appearing during each process. A multivariate analysis uncovered that (i) at Mo K-edge, activation of oxidic precursor is a 3-step mechanism with one reduced-like and one oxysulfide species as intermediates and (ii) TPR is a 2-step process with in which the reduced intermediate is a common species between the two processes. This approach was fundamental to properly number the steps during the TPR and to correctly assign the first intermediate of the activation as a non-sulfide species. Further, when applied to low loading catalyst, remarkably structural differences on the kinetics was found, but a similar active phase was reach at the end. Thereby, using augmented analyses we demonstrated that a careful planning of the experiments is essential to resolve fine details in the kinetics of the reaction.

INTRODUCTION

The world demand for clean fuel, particularly sulfur-free fuel, ruled by severe governmental policies of pollutant levels, boosted scientists to perform finer researches to get new insights on hydrodesulfurization (HDS) catalytic reaction in order to understand the mechanisms at molecular level of the process and, thus, improve catalytic performance [1]. Such optimization of formulation and improvement of performance requires a good understanding of the structure of the catalyst, its transformations during the reactions, the genesis and the nature of active species. This requires an important development or improving of *in situ* methods, particularly spectroscopy based-methods to allow us to get new insights at molecular level of the genesis of the catalytic active phase [2]. In this scenario, X-ray

absorption spectroscopy (XAS) is suitable to probe local atomic structure and the new generation of synchrotron facilities provided conditions to perform the development of spectroscopic and diffraction techniques to a high level of resolution and sensitivity which drove the implementation of such experiments in *in situ* conditions [3].

In catalysis, the properties of active surface sites depend among others on the type and number of surrounding atoms at the surface, the supporting material and the presence of reactants and products [3]. Often, the actual size and shape of the nanoparticles also determine the reactivity of the materials. This structural complexity combined with extreme reaction conditions are factors limiting the possibility of achieving a detailed structural characterization [4]. Technologically, the preparation of the HDS catalyst is a major issue, and the XAS has decisive influence on good directions for synthesis process [5]. For instance, upon adding Co in preparation of the MoS_2-based catalysts, one obtains the so-called CoMoS active species, which is essentially MoS_2 nanoparticles decorated by Co atoms [6]–[8]. A prerequisite for a thorough elucidation of this issue seems to be a better understanding of the morphology, the atomic-scale structure of CoMoS clusters or its genesis.

The so-called chemometrics tools, such as Principal Component Analysis (PCA) is one of the most basic and widely used instrument devoted to interpreting complex chemical evolution and to obtain a quantitative distribution of the chemical species contributing to those set of spectra [9]–[11]. Further, Multivariate Curve Resolution with Alternating Least Squares (MCR-ALS) fitting analysis has been implemented to get insights on chemical transformations from spectroscopy data in order to determine the reaction mechanism, which has brought a renewed perspective in analysis of the behavior of precursors, their evolution and kinetics during a given reaction [12], [13]. Such analysis is performed essentially by using a mixing of modelling method to mathematically decompose the data set of a mixture (a

reaction) into the pure contributions of the components involved in the system studied [12]–[14]. Recently, this approach has been applied successfully in the treatment of XAS-based time-resolved experiments in different systems and reactions [15]–[19].

This work is devoted to deeply discuss the methods of chemometrics applied to treat *in situ* XAS data sets. We intend to show a whole package of PCA analyses that one can use to discuss the first fundamental and crucial issue when treating reaction systems, *i.e.*, "how many components are there in the system?". The starting point of any analytic reaction modeling is to correctly address this question because, particularly in MCR-ALS, a bad choice of this parameter can lead to wrong calculated profiles and completely different interpretation of the reaction. Here, we consider Quick-XAS (also known as QEXAFS or Quick-EXAFS) data set recorded during the *in situ* monitoring of the Temperature Programmed Reduction (TPR) and the activation of a TiO_2-supported CoMo-based catalyst under reactive atmosphere, which gives rise to the formation of the active phase, a MoS_2-like structure [20]. In the first part we present a wide set of tools from PCA analysis that can be used to choose the good number of components of a reaction taking as model the well-known activation of the oxidic precursor. These findings are important to validate our analysis, which are, then, extended to TPR and to the column-wise augmented matrix on the sections that follows. Particularly, for an augmented system, we illustrate how this method can give improved results on the description of the reactions if wisely used combining complementary experiments to unravel intermediary species or to resolve the actual "quality" of a particular component. As a major consequence, one must carefully plan the experiments when trying to get fine information on evolving systems, as in catalytic activation, for instance.

On the last section, we demonstrate the power of MCR-ALS results as a tool for description the subtle differences on the evolution of the oxidic precursor with distinct Mo-loading. We

discuss how it is related to the performance of the catalyst not just by the fact of having less loading, but also in how the interaction with the support may play an important role on the structure and genesis of the active phase.

METHODS

Sample Preparation and Characterization

CoMo precursors were prepared through classic simultaneous incipient wetness impregnation (IWI), as described elsewhere [21]. A solution of ammonium molybdate tetrahydrate (AHM, with linear formula $(NH_4)_6Mo_7O_{24}\cdot 4H_2O$, ≥ 99.0%, from Sigma-Aldrich®), cobalt(II) nitrate hexahydrate (with linear formula $Co(NO_3)_2\cdot 6H_2O$, ≥ 99.0%, from Fluka/Sigma-Aldrich®) and double distillated water was used to impregnate a commercial titanium (IV) oxide with a specific surface area of 200 m²/g. The solutions were prepared in order to keep the Co/Mo atomic ratio equal to 0.5. A series of four solids with different MoO_3 loadings were prepared, the lower with 5 wt.% of MoO_3 (named as CoMo5), two intermediates with 10 and 15 wt.% (respectivelly, CoMo10 and CoMo15) and the highest loading with 20 wt.% of MoO_3 (named as CoMo20). All solids were dried in oven for one night at 100 °C and then calcined inside a reactor cell in air flux at 500 °C with a ramp of 1 °C/min for 4h. For activation, the precursor (200 mg) was placed in a reactor and a mixed gas flow (9/1 ratio of H_2/H_2S) passed through it while the temperature increased from room temperature (RT) to 400 °C at fixed rate of 6 °C/min. The sulfidation was finished after 2h at the plateau. The activity of all catalysts was evaluated in the HDS of thiophene at 300 °C and atmospheric pressure. The feed of vacuum-distillated thiophene was introduced into the flow-type reactor at constant pressure with hydrogen. The product stream was analyzed with a gas chromatograph of flame ionization detector and PLOT alumina column. Conversion values were reported after 4h of reaction [22].

All calcined samples were previously characterized by high-resolution XPS to check Co/Mo ratio as well as dispersion on the support [23], [24] and Raman (also for dispersion) [22]. A microprobe Infinity from Jobin-Yvon equipped with a N_2-cooled charge-coupled device detector was used. The exciting laser source was the 532 nm line of the Nd:YAG laser.

In situ X-Ray Absorption Spectroscopy

Time resolved *in situ* X-ray Absorption Spectroscopy (XAS) measurements were carried out with the Quick-XAS monochromator [25] available on the SAMBA beamline* at SOLEIL synchrotron [26]. This beamline is well-known for producing high quality time-resolved in situ QEXAFS data in catalysis using different setups, reaction cells and coupled techniques [27]–[29], with resolution up to ms. The Si (111) and the Si (311) channel-cut crystal were used, respectively, to measure Co K-edge and Mo K-edge.

For the *in situ* activation study with the reaction cell, samples were heated up to 400 °C in a ramp of 6 °C/min under a flux of H_2/H_2S (15% H_2S). They rested for 1h at the plateau and then were cooled down to room temperature under helium flux. The mass of each catalyst was chosen to optimize the edge-jump at the corresponding K-edge. Eventually, the catalysts were diluted with diamond powder to fill up the reaction cell cavity. For TPR, the gas flow was set to be a 5% H_2/N_2 mixture and the conditions of temperature and reaction cells were equivalent to the prior.

One spectrum (with upward angle) per second was recorded at each one of the three stages of reaction, *i.e.*, heating, plateau and after cooling. In order to improve XAS signal-to-noise ratio, we averaged each 30 spectra during the heating ramp. Thereby, one single spectrum in

* Moved now to ROCK beamline.

the data set corresponds to 30 seconds of reaction. At the plateau and after cooling down, no longer reaction neither atomic-structural changes are expected, thus we averaged each 200 spectra to form a single one. XAS analysis and EXAFS simulation were performed with the Demeter package [30].

Chemometric data analysis

MCR-ALS method consists in the decomposition of the raw data matrix of evolving spectra into bilinear contributions of the pure components, *i.e.*, concentration profile and pure spectra [12]. Details in description of the method, specially when applied to catalysis, can be found elsewhere [12], [13], [31]–[34]. Here we follow and use the MATLAB toolbox created by Tauler et al. [35] and detailed procedures adopted in this manuscript can be found in Supplementary Information (SI). Briefly, our data set matrix containing time-resolved XAS spectra, **D**, can be described as a product of pure spectra matrix (from pure species present in the reaction), **S**, and the respective concentration matrix, **C**, following the relation:

(1) $\boldsymbol{D} = \boldsymbol{C}*\boldsymbol{S}^{\boldsymbol{T}} + \boldsymbol{E}$,

with $\boldsymbol{E}$ the residual matrix. The method consists in wisely choose the correct rank k of matrices **C** and **S**, then build an initial guess for one of these matrices and then refine by minimization processes with respect to the data set **D**. At the end, our reaction can be described dynamically by k species with pure spectra given by matrix **S**, evolving according to concentration profile **C**. PCA is used for choosing the rank and to construct the initial guess, while MCR-ALS algorithm "tailors" **C** and $\mathbf{S^T}$ according to the chemical properties and the mathematical features of each particular data set, **D**. Singular Value Decomposition (SVD) algorithm was used for PCA analysis with calculation of the elements to be consider in rank choice, such as, eigenvalues, score matrix and loading matrix. Constraints in MCR-ALS (e.g.,

non-negativity, unimodality, closure, etc.) as well as local rank and selective windows were used to fit calculations to physical meaning of each reaction. The flexibility in 'where-and-how' applying constraints and the capability to treat the most diverse multiset structures are the main assets of this algorithm. The 'art' and expertise in using MCR-ALS stems from the proper selection and application of the constraints that are really fulfilled by the data set and from the ability to envision how to design and to deal with the most informative multiset structures.

Three matrices were separately analyzed for each sample: the matrix containing TPR data, the matrix containing activation data, and the so-called column-wise augmented matrix, where TPR and activation data were gathered in one single matrix. Chemometric analysis was performed in 2 samples of our series, the highest and the lowest Mo-loading solids, respectively, CoMo20 and CoMo5.

RESULTS AND DISCUSSION

Characterization of Oxide Precursors and *in situ* XAS

Raman spectra of calcined oxide precursors exhibit mainly anatase-TiO_2 lines, but also indicates a good dispersion of the polymolybdates species on the support surface [21], [36] (Figure S01), which was enough to assume single component/structure at the start of the reaction. Regarding the catalytic performance, a typical evolution of the conversion versus the molybdenum loading was observed, with a gradual increase until a plateau was reached (Table S1).

Figure 1 shows Mo K-edge XANES from *in situ* experiments of both activation and TPR of the catalyst with higher Mo-loading (20 wt.% of MoO_3), namely CoMo20. Initial species are

the same in both cases (from the same synthesis) and our goal is to describe their evolution in each case. A visual inspection shows the main spectral features changing during the reaction. For instance, during activation (Figure 1, top), the oxidic precursor passes through changes at the beginning of the reaction, still at low temperatures. We observe the third XANES bump diminishing (~ 20070 eV) followed by pre-edge feature that vanishes and then the progressive rising of the shoulder (~ 20010 eV) typical of the MoS_2 phase, as indicated by the arrows (respectively, numbers 1, 2 and 3). During TPR instead, changes occur at high temperature regime (Figure 1, bottom). First, we observe the quenching of the pre-edge peak and the XANES bump around 20055 eV (Figure 1, bottom, arrows 1) followed by the rising of the pre-edge feature typical of reduced species together with a bump around 20090 eV (arrows 2).

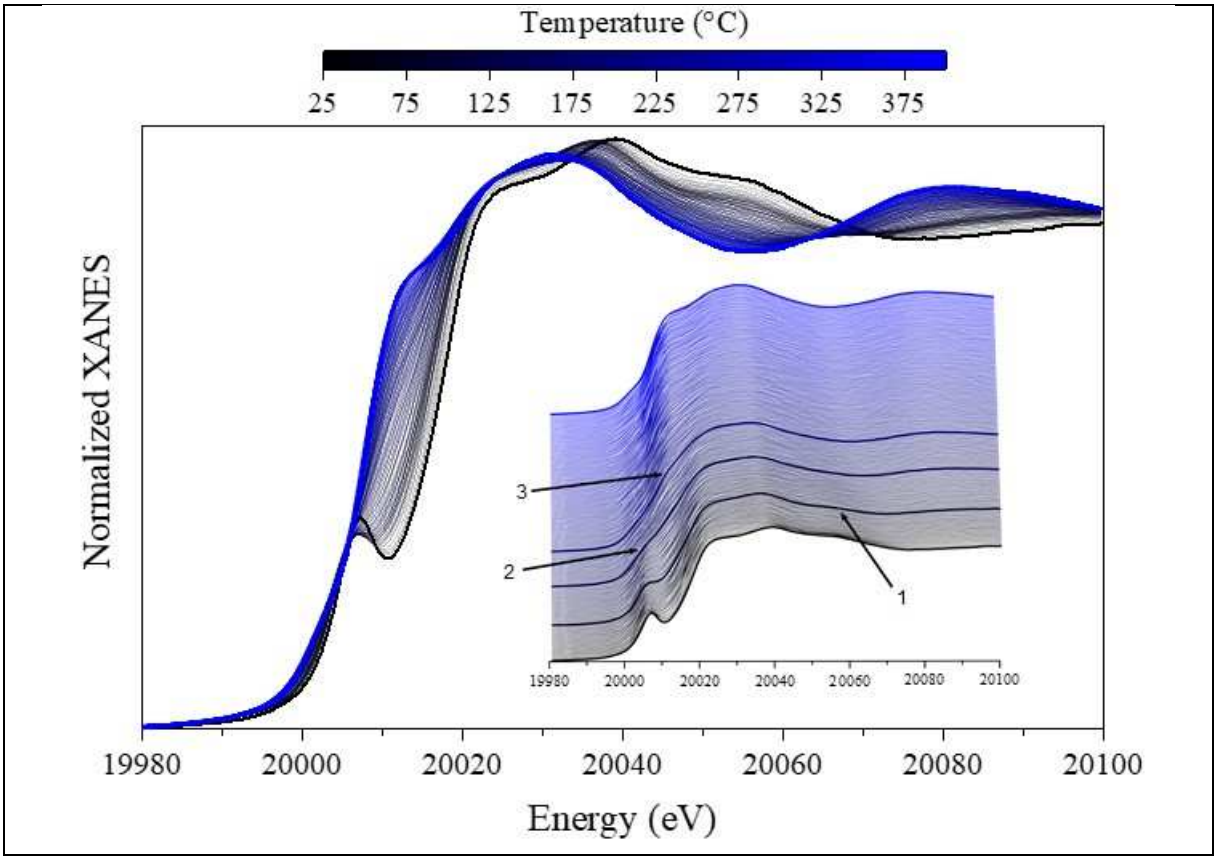

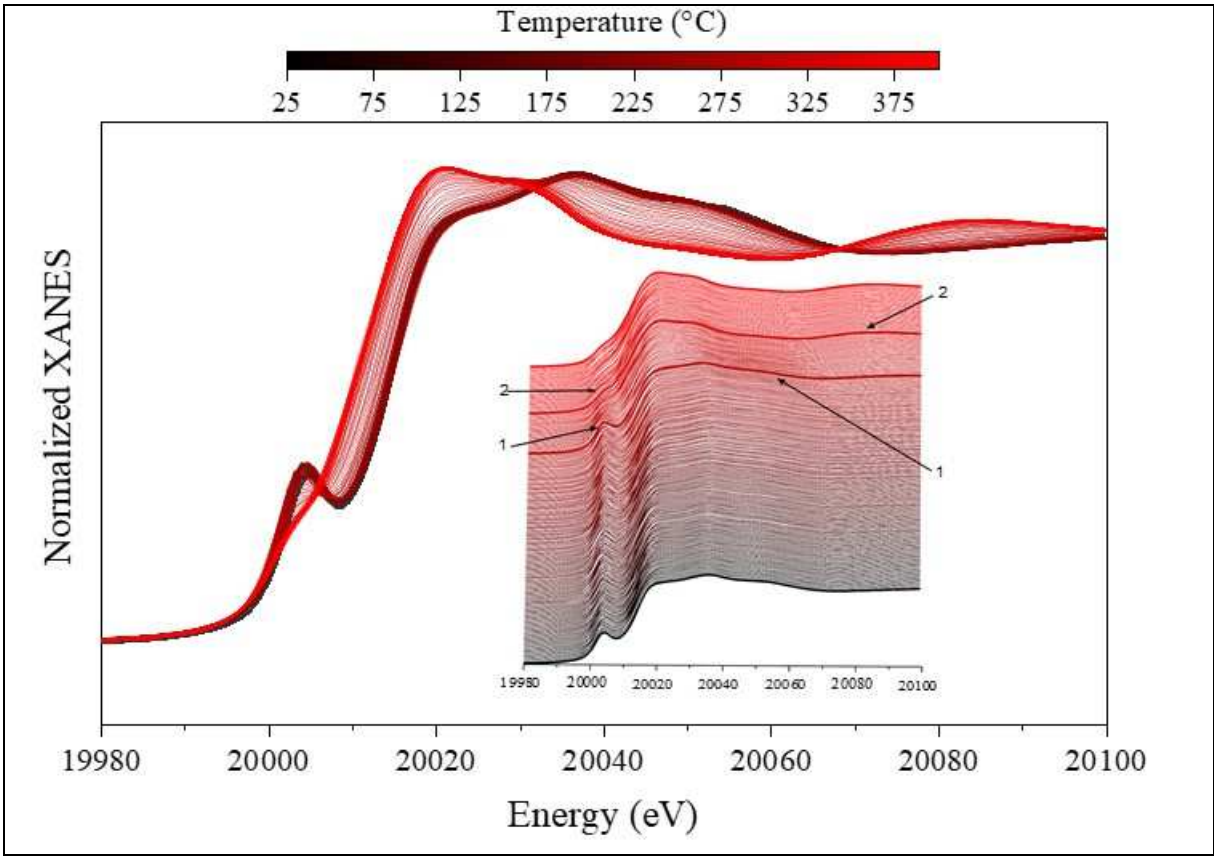

Figure 1 - Mo K-edge XANES evolution of CoMo20 during activation (top) and TPR (bottom).

Since these isolated features are the result of the combination of different "pure" species spectra, Chemometrics is a suitable tool to get insights on the kinetics of the reaction and on the description of the structural/chemical transformations. This approach requires to write the data set in a matrix, in which each row represents a whole XAS spectrum in a particular time, *i.e.*, a snapshot of the reaction. In that sense, we built one matrix for each reaction. A third one was built gathering data from two independent experiments in one single matrix, the so-called, column-wise augmented matrix. Then, we apply chemometrics to extract information related to the number of chemical species present in each reaction, their respective pure spectra and the concentration profile. In other words, we calculate the Principal Components by SVD for each matrix and wisely chose the number of PC's to be considered.

Chemometric Approach for time-resolved in situ XAS data

The following sections are dedicated to discuss XAS data. As stated before, we have used chemometric tools to treat the whole time-resolved *in situ* data set. Structural analysis of oxide precursor, which could be performed by *ex situ* measurements, will come naturally with the rest of the analysis, since it is supposed to be a "single initial species". Actually, how it was pointed out early by Rochet *et al* [19], this initial species is composed by different Mo-oxydic ones, but concerning the XAS point of view (also for MCR-ALS) we treat it as a single phase.

a) The Choice of the Number of Components

SVD was applied separately on the three matrices, namely, Reduction, Activation and Column-Wise Augmented dataset. The results are independent for each matrix and they are gathered in a table showing the calculated eigenvalue and the variance explained by each Principal Component as well as the cumulative explained variance for the nine first PC's (Table 1). As stated before, a major issue is to choose a criterion to stop the PC counting (as, for instance, the statistical stopping rules summarized by Peres-Neto [37]). In other words, we are looking for a threshold below which the explained variance assumes a negligible value. Unfortunately, a foolproof method for automating the choice has yet to be discovered. Instead, the choice must be made based upon a few rules of thumb and, mainly, the knowledge of the data and chemical reaction by the scientists.

Taking CoMo20 dataset at the Mo K-edge as a model, the raw *in situ* TPR data is a matrix with 214 rows and 539 columns (containing the energy value). In order to minimize the noise effect to the chemometric calculations all the region before pre-peak was ignored (about the first 100 points of each spectrum). Following the same argument, CoMo20 activation matrix is a (199,425) size and column-wise augmented CoMo20 system is a (413,425) matrix.

Table 1 contains the results from SVD calculations for the three considered systems. It can be used to establish the suitable number of PC's by considering a certain threshold below which we can neglect the PC contribution. Say, for instance, 1% of variance explained. In reduction experiment the first PC explain 95.7% of the data, the second PC explain 2.43% of the data (and the cumulative variance explained goes to 98.16%), the third PC explain 0.27% of the data (with 98.43% of cumulative variance explained). From third PC on, each new PC is responsible to explain a worthless part of the data, namely, less than 1% (see also the cumulative variance explained), and thus we may assume that 3 PC's is enough to describe the whole data set. Adopting this criterion, all three considered matrix systems would have three components (yellow-highlighted on Table 1).

Table 1 - SVD results for CoMo20 matrices.

	Reduction			**Activation**			**Augmented System**		
PC	Eigenvalue	Var. Expl.	Cum. Var. Exp.	Eigenvalue	Var. Expl.	Cum. Var. Exp.	Eigenvalue	Var. Expl.	Cum. Var. Exp.
1	288.810	95.70	95.70	279.503	95.96	95.96	401.812	94.00	94.00
2	7.33853	2.43	98.16	6.82244	2.34	98.30	12.8970	3.02	97.02
3	0.82408	0.27	98.43	0.81838	0.28	98.58	3.84998	0.90	97.92
4	0.56335	0.19	98.62	0.34820	0.12	98.70	0.95519	0.22	98.14
5	0.33626	0.11	98.73	0.19192	0.07	98.77	0.61645	0.14	98.29
6	0.19887	0.07	98.80	0.14329	0.05	98.81	0.43920	0.10	98.39
7	0.17744	0.06	98.86	0.13533	0.05	98.86	0.40567	0.09	98.48
8	0.15651	0.05	98.91	0.09746	0.03	98.89	0.22930	0.05	98.54
9	0.11256	0.04	98.95	0.09208	0.03	98.93	0.18404	0.04	98.58

* Values of Variance Explained and Cumulative Variance Explained are given in %

Another threshold that could be adopted is to consider the difference in magnitude of a certain eigenvalue to the next one. We consider the PC's until the difference between the nth PC and the $(n+1)^{th}$ PC tends to zero (the green highlighted values on Table 1). As an example, yet in reduction results, one observes that from PC 1 up to PC 5 the difference between the

eigenvalue and the next is not negligible (the difference between PC 5 and PC 4 is 0.23). From PC 6 on, this difference tends to zero (PC 6 - PC 7 = 0.19 - 0.17 = 0.02) and, thus, PC 6 is out of our criteria. In this scenario, reduction would have five pure compounds; activation, four pure compounds; and the augmented system, 7 (or even 8) pure compounds.

Alternatively, we may look at eigenvalues for a matrix data set by its scree plot, or log scree plot (Figure 2). Since the first eigenvalue is much larger than the following ones, we can either plot the logarithmic of the eigenvalues against the PC number (inset of Figure 2) or exclude the first PC from the ordinary plot. From the figure, while reduction and activation point to 3 PC's each, the augmented system suggests at least 4 PC's. The analysis of logarithmic plot is ambiguous because the "elbow" is not obvious. This mismatch between the two criteria (reinforced by the scree plot) indicates that a precise choice of the number of PC's is not straightforward. Then, we will explore further results from SVD decomposition in order to make a confident choice on the number of significant components necessary to describe each dataset.

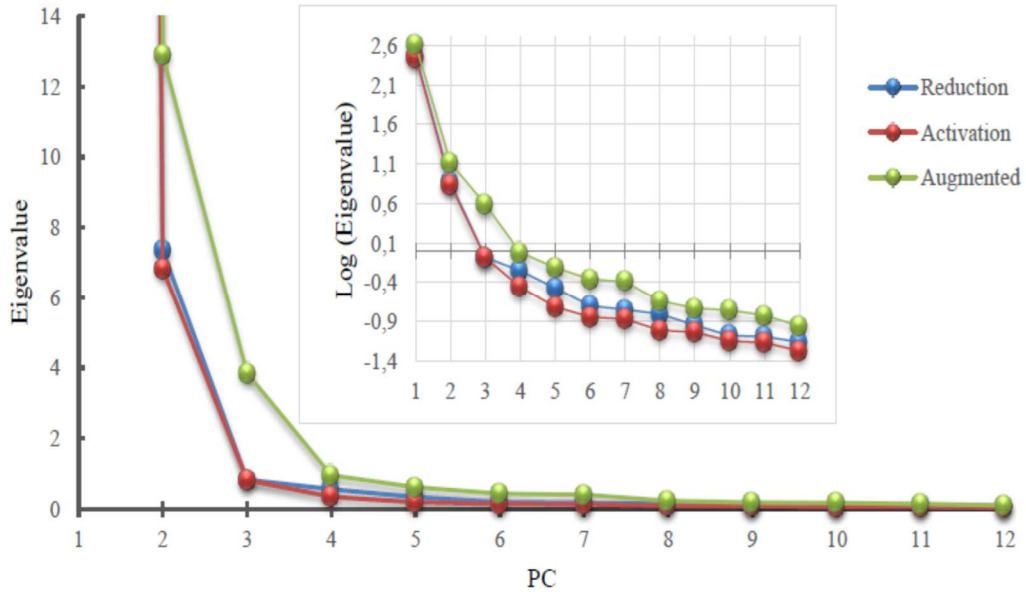

Figure 2 - Scree plot for CoMo20 system. The inset shows the log scree plot.

In the SVD decomposition of any matrix, we obtain three new ones: the eigenvalue matrix, the loading and the scores ones. The last two can be viewed, respectively, as the new set of basis vectors for our data and the projections of the experimental data onto this new orthonormal and linearly independent set of basis [38]–[40]. In the following, we present a suitable interpretation to the PCA method (especially, loading and scores matrices) taking as example the activation matrix. It is worth noting that we have several results from PCA to interpret, which will be separately discussed below, and it is the whole set of individual conclusions will lead us to the wise choice of number of PC's.

Loading matrix contains the new basis, or the eigenvectors, mathematically built in terms of variance of the experimental data set matrix. In that sense, the first vector (or the first PC, in terms of loading matrix element) can be regarded as the average of all spectra of the data set, as showed in Figure 3. (Special attention must be taken when looking this construction. Besides its great similarity with a XAS spectrum, it is actually calculated to minimize the variance of the data set.) By plotting the other vectors, and taking into account the respective eigenvalues and the variance explained, we can check the relevance of each one to describe the variance of the data set. Thus, we can attribute an arbitrary relevance to that PC. These components are plotted weighted by its respective eigenvalue, but we can look at the non-weighted plot (Figure S02) to check how noisy (and thus, less representative) is a particular component. By visual analysis, it seems that at least the three first PC's have some importance, but it seems to be not enough to judge how representative are PC 4 and 5 to the data.

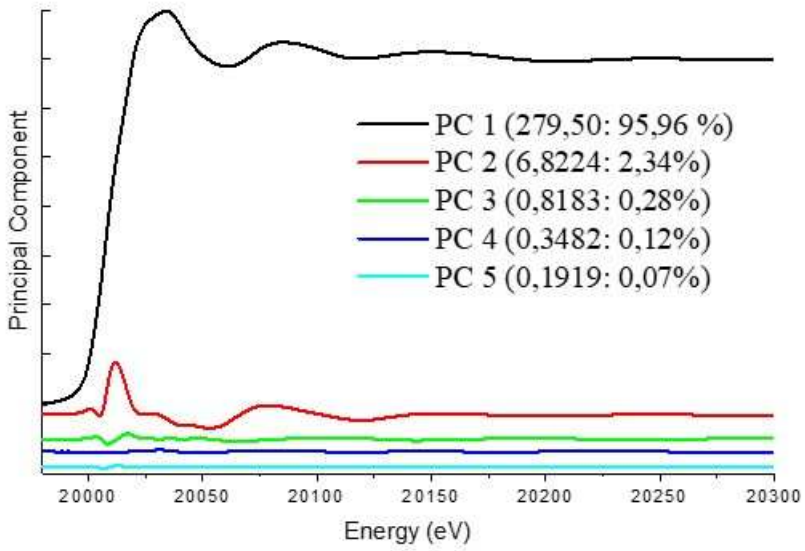

Figure 3 - Loading plot: the 5 first elements (Principal Components) of loading matrix related to the activation data set of CoMo20. In parenthesis, respectively, the eigenvalue associated to that PC and the variance explained.

Turning to the score matrix, its elements tell us how the eigenvectors "evolve" throughout the data set, acting as a kind of "weight" for them. Figure 4 show us the "evolution" of scores referent to the same data set of Figure 3. Looking how they evolve during the "reaction" can tell us the importance of each one for describing the experimental data. The more randomized is the shape of score line (related to a certain PC), the more this PC is irrelevant as a valuable component. Thus, we interpret Figure 4 as follows: the first PC is related to the presence of the first element (the first vector of the basis) of the loading matrix. Since it represents the average of all spectra, it should be equally present in every point of the score representation. Therefore, it must be a straight line parallel to x-axis (top black line in Figure 4). The rest of the components have their own individual behavior, but by visual inspection we can surely state that the fifth element has a completely random behavior and can be attributed to nothing but noise of the data. Consequently, we have strong evidence to establish 4 as being the maximum number of principal components necessary to describe our experimental data set. It is worth noting that the components in Figure 4 ant their behavior are mathematical

constructions in the context of the SVD decomposition and must not be interpreted as true species evolving during the reaction.

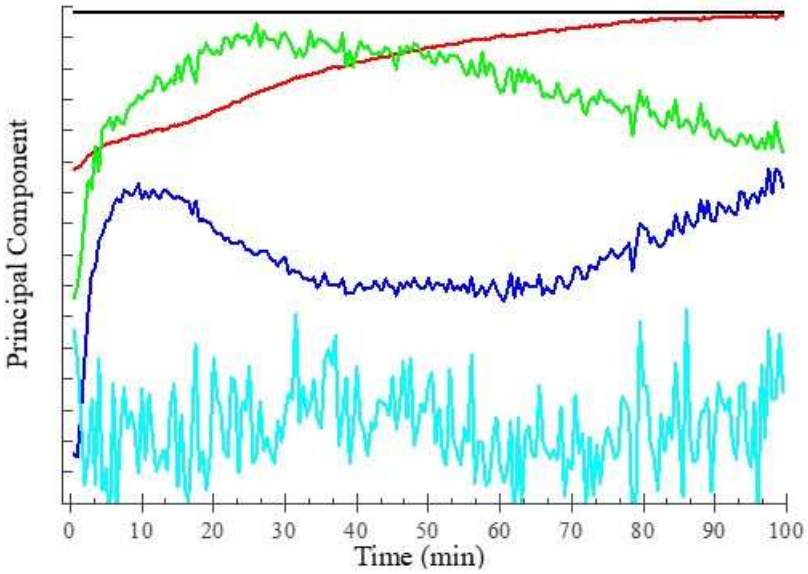

Figure 4 - Evolving score plot: the 5 first elements of score matrix referent to activation data set of CoMo20. The color code is the same as in Fig. 4.

Despite all these evidences, we may eventually handle data sets that are not so easy to make a clear conclusion. Data from TPR is a good example on that issue and the examination of its PCA results are shown latter on this manuscript. Thus, we present briefly two additional tools that are useful to gather more evidences concerning the number of PC's to be considered. (Further details are included in SI.)

The first tool is examining the plot of the residual after the reconstruction of experimental data considering different numbers of PC's [17], [32], [41] (discussed in more details on the next section). Briefly, starting with 2 PC's, we perform inverse mathematical operations to reconstruct the experimental data. The difference between real data and reconstructed one is the residual (equation 1). The more components we include, the smaller is the residual, up to a

limit where an additional PC does not add any further information in description of experimental data (see TPR analysis below as example of this tool).

The second is to construct 3D scatter plots of the score matrix, as showed in Figure 5. This mapping method may reveal groups of samples[†] (clusters); indicating a same (or closely related) chemical species, or paths, which are related to chemical transformation in a certain species $A \rightarrow B$. Briefly, each instantly recorded experimental spectrum has its components in the new basis vectors, which is given by the score matrix. Two samples with similar components are closely related, i.e., its representation in the n-dimensional "score space" are also close together. In a chemical reaction, we expect a gradual structural transformation from one species to another. In such representation, it means a straight line from one point to another. This picture is illustrated in Figure 5 for the activation of CoMo20. We have a 3D "score space" formed by the SVD-calculated scores of PC1 x PC2 x PC3 (Figure 5a). This curve may be interpreted as 2 connected straight lines, which means a 2-step chemical transformation, or $A \rightarrow B \rightarrow C$. Since we want to test the others calculated PC's, we draw another 3D projection, now with PC1 x PC2 x PC4 (Figure 5b). This representation seems to describe even better our system, we identify 4 vertices in the figure, which can be interpreted as a 3-step reaction. By checking if PC5 gives further information, we observe that its corresponding 3D representation (Figure 5c) presents a random feature (projected in PC2 x PC5 plane). This strongly suggests that PC5 is not a valuable principal component for our system and we have indeed 4 PC's.

[†] In chemometric language, a sample is a row in the data set matrix. In practice, it is a recorded snapshotted spectrum.

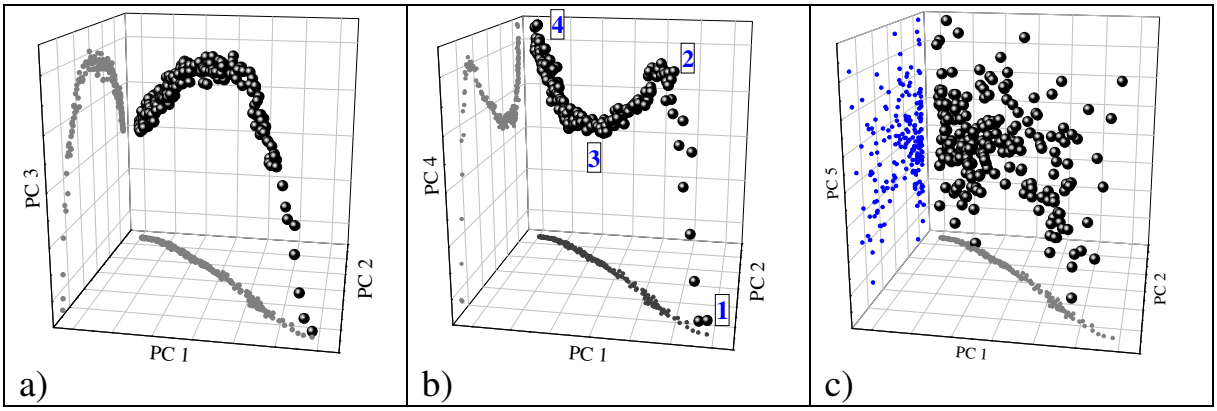

Figure 5 - 3D scatter plot of scores obtained from activation matrix of CoMo20 in different configurations of z-axis.

Thus, we have seen that a proper way to interpret PCA results passes by the complementary analysis of scores and loading plots, residual from reconstructed data and variance explained. Concerning our activation dataset, in particular, the tools that offered more evidence for the choose of the number of components were the evolving score plot and the scatter plot of scores, respectively, Figure 4 and Figure 5, pointing to 4 PCs. We, then, should consider a range of possibilities for each data matrix for MCR calculations and the (XANES/EXAFS) analysis of the pure components will dictate the accuracy of the choice. In other words, this is an iterative problem. Further, a good knowledge of the reaction is somehow fundamental in the course of component choice and for this kind of system (activation of CoMo-based catalyst), we do expect something such as a 3-step process, as exemplified elsewhere [19]. Therefore, 4 PCs was our wise choice.

b) Pure Spectra and Concentration Profiles calculated by MCR-ALS

MCR-ALS method requires an initial guess of spectra or concentration profile as an entry for the calculations (see SI for details). For each data set and MCR calculation, we also performed tests using different combinations of constraints. When applied on Mo K-edge XAS activation matrix, it gave us solid results when setting 4 PC's and using simple

constrains such as, non-negativity in concentration profile and spectra, unimodality and closure constrain in concentration profile (Figure 6).

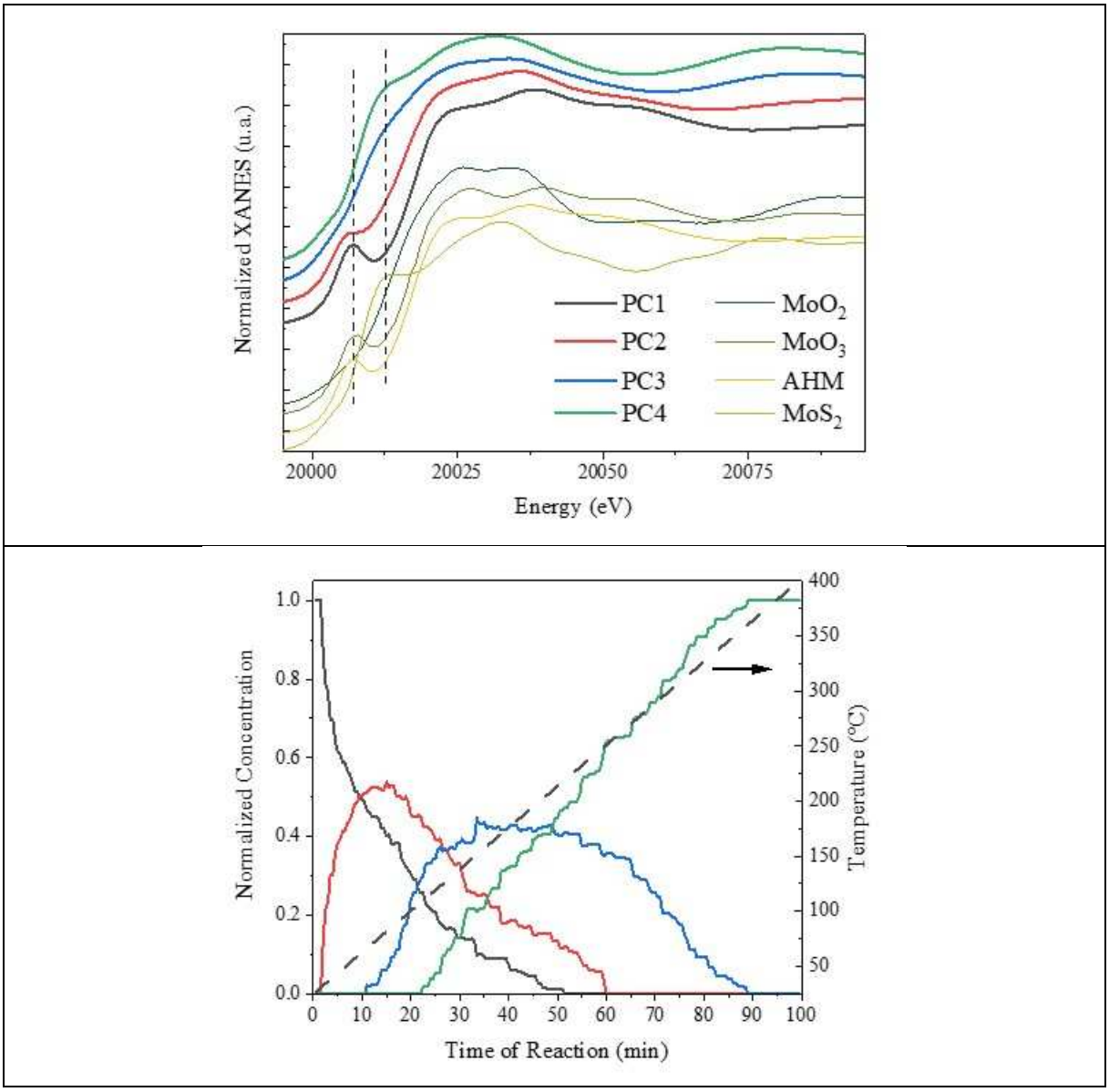

Figure 6 - (Top) MCR-ALS pure spectra (Mo K-edge) stacked with references (dashed lines are visual guides) and (bottom) concentration profiles for activation of CoMo20 calculated with 4 components.

Qualitative interpretation of the activation reaction of the CoMo20 catalyst is, then, straightforward (Figure 6, bottom): the precursor oxide (PC1) transforms completely into active phase passing by two intermediates species. The first one (PC2) starts to rise early at

very low temperature (before 50 °C). The second one (PC3), appears a dozen minutes after (about 100 °C), when the first intermediate achieve its maximum concentration level and, then, starts to fall. Final state (PC4) starts to be formed about 22 minutes along the reaction, in a temperature slightly below 150 °C. From 90 minutes on, at 350 °C, all precursor is converted into final state and the transformation is completed.

MCR-ALS procedure gave us individual component spectra that can be processed as conventional XANES and EXAFS spectra. In Figure 6 (top), oxide precursor (PC1) is in the same oxidation state as MoO_3 (formally, Mo^{VI}), adopted as reference. PC4 has all features of MoS_2, the active phase, adopted as reference and a formal oxidation state of Mo^{IV}. PC 2 still has features of an oxide, such as the pre-peak, but it does not seem to be a completely reduced oxide (by visual comparation with the features in MoO_2 spectrum) and PC 3 presents XANES-sulfide features, like a kind of proto-shoulder around 20020 eV, typical of bulk MoS_2. The real nature of these two intermediates should be puzzled out with EXAFS analysis, which is discussed in the following.

Structural information obtained from EXAFS procedure for each species are gathered in Table 2. Some features can be highlighted in EXAFS results, Figure S03 shows the Fourier transform calculated from Mo K-edge EXAFS of MCR-ALS components (without phase correction). PC 1 in Figure 6 is the precursor oxide specie, the peak centered at 1.85 Å corresponds to short and long Mo-O contributions, typical for such oxides. Two Mo-Mo distances consistent with those found for polymolybdates such as AHM, i.e., $(NH_4)_6Mo_7O_{24}$, and one Mo-Co contributions could be satisfactory simulated. Actually, even if the XANES features of our precursor oxide is very close from that of AHM, as shown clearly on Figure 6 (top), likely it is formed by a mixture of different oxide species, among them, an Anderson-type heteropolyanion ($AlMo_6$) or a dimeric molybdate $(NH_4)_2Mo_2O_7$ [19]. The low N_{Ti}

simulated feature is consistent with a Mo-O-Ti bridge as found in similar systems [42], which may be interpreted as a weak interaction with support instead as properly a chemical bond. PC 2 in Figure 6 is the first intermediate (the Partially Reduced in Table 2). Figure S03 (right panel) shows the evolution of the system from Fourier Transform analysis. We satisfactorily simulated one Mo-O bond and one extra short Mo-Mo contribution similar to those found for reduced Mo species (as in MoO_2). This pure component has features from both, oxidic and reduced species, thus we call it Partially Reduced species. No Mo-S contribution could be properly simulated, suggesting that the oxide precursor evolves to a reduced species as first step of the activation. Actually, this interpretation gained force after we check that the PC2-EXAFS is very similar to a selected spectrum (not the last one, since it is clearly not a reduced Mo) from the experimental dataset of TPR (Figure S09) It suggests further that, at this point of the reaction, both H_2 and H_2S are (consumed and) used as reducing agents [28]. High correlation among the fit parameters (mainly between path degeneracy and sigma square) prevented us to find coordination number (N) values with narrow error bars for metal-metal contributions.

Intriguingly, we expected to obtain as a first intermediary an oxysulfide species, as demonstrated earlier by Weber *et al* [43] and recently proposed by Rochet *et al* [44] for Mo-based catalysts supported on alumina. However, we have to keep in mind that different Mo precursor and a distinct support may lead the reaction to another path of evolution.

Table 2 - Fitted Parameters of CoMo20 species at Mo K-edge (E_0 = 20004 ± 1 eV, S_0^2 = 0.96) and Co K-edge (E_0 = 7709 ± 1 eV, S_0^2 = 0.85)

Backscatterer	*N*	*σ² (Å²) x 10⁻³*	*R (Å)*
Mo K edge			
Precursor Oxide			
O	3.5 ± 0.6	5 ± 1	1.746 ± 0.005
O	1.5 ± 0.4	5 ± 1	1.96 ± 0.01
Ti	0.2 ± 0.1	4 ± 2	2.73 ± 0.03
Mo	0.8 ± 0.2	2 ± 2	3.26 ± 0.01
Mo	0.8 ± 0.2	2 ± 2	3.39 ± 0.01
Co	0.8* ± 0.2	4 ± 2	3.88 ± 0.02
ΔE = 0 eV, r-factor = 0.013, χ^2 = 465, N_{ind} = 16, N_{var} = 12			
Partially Reduced			
O	2.3 ± 0.8	4 ± 4	1.99 ± 0.01
O	2.3 ± 0.8	4 ± 4	2.06 ± 0.02
Mo	0.6 ± 0.9	7 ± 7	2.58 ± 0.03
Mo	0.6 ± 0.9	7 ± 7	3.25 ± 0.06
Mo	0.6 ± 0.9	7 ± 7	3.36 ± 0.07
Co	0.9 ± 0.4	3 ± 3	3.97 ± 0.05
ΔE = 3.2 eV, r-factor = 0.021, χ^2 = 1801, N_{ind} = 12, N_{var} = 11			
Reduced Oxide			
O	1.8 ± 0.6	1 ± 3	2.01 ± 0.03
O	1.8 ± 0.6	5 ± 9	2.49 ± 0.01
Mo	0.7 ± 0.1	4 ± 2	2.60 ± 0.02
Mo	0.7 ± 0.1	4 ± 2	3.17 ± 0.04
Mo	1.0 ± 0.1	4 ± 2	3.33 ± 0.04
ΔE = 3.2 eV, r-factor =0.029, χ^2 =2494, N_{ind} = 12, N_{var} = 9			
Oxisulfide/MoS_3-like			
Fit Oxisulfide			
O	1.1 ± 0.4	8 ± 4	2.01 ± 0.02
S	1.8 ± 0.7	8 ± 4	2.37 ± 0.01
Mo	0.6 ± 0.1	12 ± 10	3.25 ± 0.08
Fit MoS_3-like			
S	3.6± 0.7	15 ± 3	2.36 ± 0.006
Mo	0.6 ± 0.1	12 ± 7	3.24 ± 0.06
ΔE = 4.0 eV, r-factor = 0.01/0.02, χ^2 = 2302/1223, N_{ind} = 10, N_{var} = 7/5			
Active Phase			
Fit A			
S	5.5 ± 0.3	4.5 ± 0.5	2.409 ± 0.002
Mo	3.2 ± 0.6	4 ± 1	3.170 ± 0.004
Fit B			
S	5.6 ± 0.4	4.5 ± 0.6	2.409 ± 0.002
Mo	3.0 ± 0.9	4 ± 1	3.170 ± 0.005
Co	0.1 ± 0.3	4 ± 1	2.9 ± 0.2
ΔE = 6.5 eV, r-factor = 0.005/0.005, χ^2 = 519/734, N_{ind} = 12, N_{var} = 6/8			
Co K edge			
Precursor Oxide			

*fixed relationship coordination numbers according to nCo = α*nMo, with α extracted XPS results.

For the second intermediate (Oxisulfide/MoS_3, in Table 2), as the main MoS_2 peak could be found during the reaction (red arrow in Figure S04), we simulated one Mo-S contribution typical of the active phase, at 2.36 Å, and one Mo-Mo contribution at 3.25 Å. It is worth to note that in similar works, for instance, that from Rochet *et al* [19], a MoS_3-like structure was proposed as an intermediate just before the active phase. And in reality, our XANES (PC3, in Figure 6, top) has a great similarity comparing to that one published for amorphous MoS_3 [45]and, particularly, we see no longer the pre-edge feature typical for oxides. Thus, we simulated 2 models for the EXAFS, with and without the Mo-O contribution, respectively on Table 2, Fit Oxysulfide and MoS_3-like. Both models are quite good concerning the statistic parameters, with a lightly favor to the MoS_3-like one, even if it presents larger σ^2 values and larger correlations among the parameters. However, we have imposed a fixe correlation for the coordination number between S and M on this model (a ratio 1/6), which was not the case of oxysulfide model. Oxysulfide model suffers from quite low Oxygen neighbors. Finally, in both models the Mo-Mo contribution is longer than expected, being closer from the MoS_2 (3.17 Å) phase instead of 2.80 Å as found on the literature (for instance, [19]).

The active phase is comparable with the experimental spectra of the bulk MoS_2 compound (the XANES in Figure 6, and FT in Figure S04). Here we also proposed two different fits, one with just Mo-S and Mo-Mo contributions (Fit A, in Table 2), like in a MoS2 structure, and other where we sought for a Mo-Co contribution (Fit B, in Table 2). The inclusion of this bond does not really improve the fit (both are comparable), even if it was found on an expected distance comparing with those found on the literature. A small N_{Co} may also suggest that Co atoms are decorating just some edges of the MoS_2 slabs. Nevertheless, we have not a robust argument from Mo K-edge that guarantee the formation of CoMoS active phase.

Further, it is worth to note that the small N_{Co} number and the MCR performed on Co-XANES (on SI) points that just a small part of cobalt atoms is used to form this (eventual) CoMoS phase, while the remain turns to Co-oxide as well as individual Co-sulfide species (see discussion on SI). These finds for the activation, particularly, a (not totally) reduced species as a first intermediate instead of an oxysulfide, motivated us to carefully study also the TPR at Mo K-edge (Figure 1, bottom).

c) MCR-ALS results for TPR and column-wise augmented matrix

When calculations are performed for TPR using its corresponding single matrix, MCR-ALS results are consistent (in terms of convergence of calculation) only for 2 principal components, despite PCA could suggest 3 components (see details in SI). Considering 2 PC's, MCR-ALS interpretation is straightforward: a single step transformation, in which the oxide precursor turns to a reduced species, which has structural similarities to MoO_2 (Reduced Oxide on Table 2 and Figure S09, bottom). However, two PC's is not enough to explain the whole data set, a s indicated by the residual plot (Figure 7). It is also clear that the fourth and the fifth PC's do not contribute to a better description of the data, since they have same average level of residual, about 3×10^{-6} (while PC3 is about 8×10^{-6}). Such residual plot also reveals where the third species (in that case) should most contribute to describe the data around the peak. That is because in a system with three components, the first two represent more than 98% of the total variance (see Table 1), thus, the higher mismatch with the experimental data appears at the time when this third species is dominant. As discussed, for example, by Cassinelli *et al* [17], this comes from building of PCA components. As they are sorted considering the variance of the data, first component (essentially, the average of all samples) represent more than 95% of such variance, while the succeeding components are

small fluctuations concerning the first one. From Table 1, we observe that the second component counts to 2.4% of the variance explained and the third one just 0.3%. Thus, in this case, such third component is suggested to be a short-lived species, with it is mostly influent exactly in the region where two components are not enough to describe correctly the data, i.e., around 70 minutes of the reaction. Supplementary Information contains further arguments that support 3 PC's consideration.

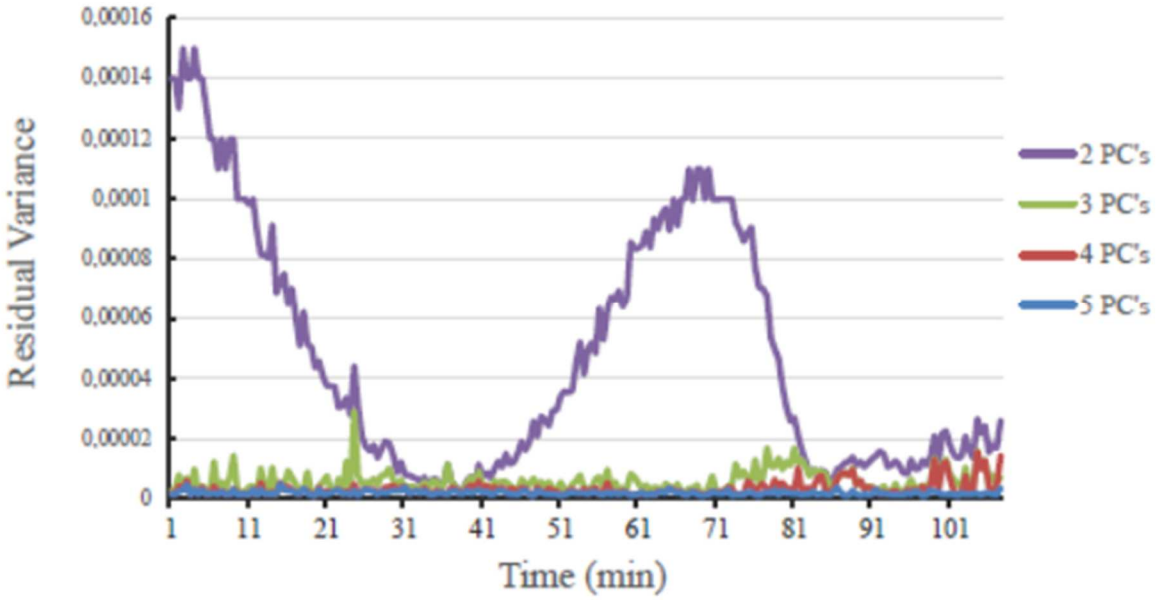

Figure 7 - Residual plot for TPR single matrix data of CoMo20 obtained from reconstruction (equation 1) of experimental data considering 2, 3, 4 and 5 PC's.

Allied to the discussion above, we recall that during activation we found a first intermediate that the EXAFS was very similar to an experimental spectrum from TPR. Thus, this is a robust motivation to apply column-wise augmented matrix in MCR-ALS calculations. By doing so, we expect to check/confirm that both reactions share a common intermediate species, by one hand, clarifying the real nature of the first intermediate in activation and by the other hand, properly quantifying the steps during the TPR.

The used protocol to choose the good number of principal components in this case must obey the same criteria previously discussed (details are found in SI). Particularly, 3D scatter score plot indicates the straight relationship between activation and reduction (Figure 8). Summarily, we decided to preserve the 4 components from activation, and count 3 for TPR. Since the oxide precursor is the same for both and we want to check if those independent reactions have one species in common, the total number of principal components to be considered in the column-wise augmented matrix is 5.

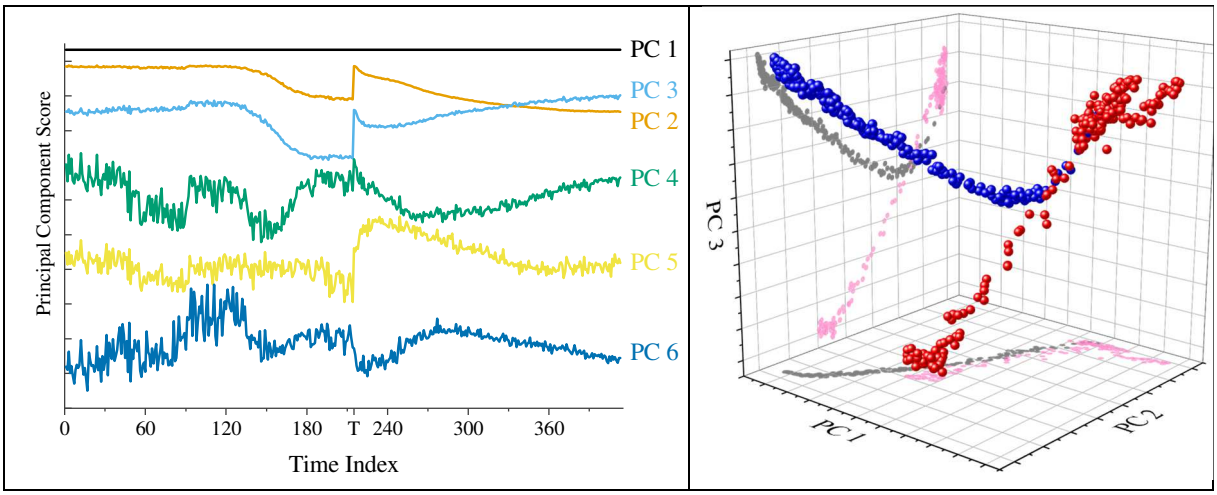

Figure 8 - (right) Scores plot for column-wise augmented CoMo20 matrix and (left) 3D scatter score plot. In scatter plot, red points are related to TPR matrix, while blue ones to activation.

Our suspicions were confirmed by the concentration profiles resulted from the MCR-ALS calculations (Figure 9), where an intermediary structure in common was found in both reactions (red curve). The concentration profile of activation is satisfactorily reproduced (comparing with analysis of single matrix), which reinforces to validate the results. It is interesting to observe that temperature of formation of this so-called partially reduced

intermediate is different when comparing the two reactions. While in TPR it starts to be formed at 270 °C (after 65 minutes of reaction), in activation it arises at room temperature some minutes after the beginning of the reaction. It appears that H_2S is a reducing agent at lower temperature than H_2. Breaking a H_2 bond is far more difficult than a H_2S bond [46], then, activation environment offers conditions to Mo-species be reduced at lower temperatures. Moreover, and quite interestingly, our results using augmented systems showed that the single MCR-ALS on TPR was not necessarily a rank deficient issue. The overall analysis, as discussed above, was not quite clear concerning the good number of principal components, although (mainly) the residual plot (Figure 7) strongly indicated the need of a third PC. Accordingly, the convergence on the calculations were not achieved in any terms using such 3-PC model, an issue that was overcame when using complementary data from activation, i.e. column-wise augmented matrix. Based on our quite recent experience on this topic, particularly on Co-based catalysts [47], [48], we are incline to state that if one has a bad hypothesis concerning the number of principal components but at a certain point one is familiar in recognize the species that evolve, then one will promptly realize the bad choice made since the resulted spectra won't be as expected (particularly on the XANES, where for certain cases one has quite different spectra, as in case of Co metallic, CoO, Co_3O_4, etc.). A major issue lies on the situation where one is completely ignorant concerning the actors present on the reaction, which is often the situation regarding HDS catalysts. On this scenario, the best chance one has is to reasonably perform EXAFS simulations for the data set in a way that could support your hypothesis for the observed evolving systems. By reasonably we mean that we are able to obtain, as solution for the fit of the considered model, structural parameters that are not so different regarding those already observed in literature for the same or similar systems. In other words, the key point is to be able to identify directly or indirectly,

the principal components regarding the structures, which is essentially the report we have been made above.

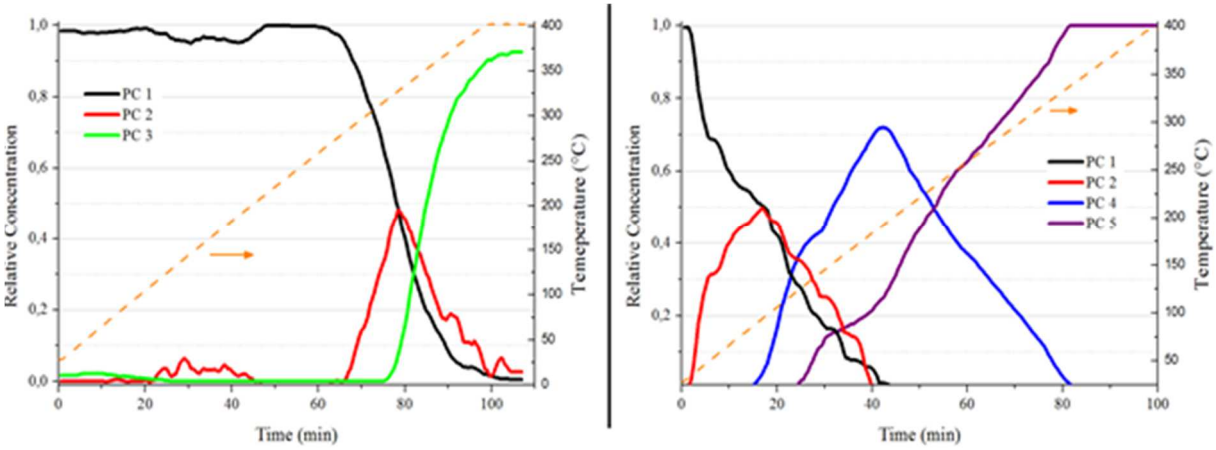

Figure 9 - MCR concentration profiles for CoMo20 augmented matrix @ Mo K-edge, left results for TPR and right, for activation.

d) Comparison with the low Mo-loading catalyst

A similar time-resolved *in situ* XAS experiment and chemometric analysis was performed for a catalyst with low Mo-loading, namely, CoMo5 (5 %wt. of MoO_3). We have seen so far, on high load catalyst, that activation occurs with the formation of 2 intermediates, the first being an oxide whereas the second being an oxisulfide species. Concerning TPR, the process is taken with the formation of one "short-lived" intermediate. At the end of both processes we have virtually a single species. It would be fruitful to check if the catalytic conversion presented in Table S1 is due simply to the lower amount of Mo species available to be converted in active phase (compared to CoMo20) or if the genesis of active phase plays a role in its efficiency.

PCA analysis was performed analogously to CoMo20 discussed above and details are provided in Supplementary Material, based on the results discussed on the previous sections,

we chose to use directly the augmented system to analyze CoMo5. As in previous experiment, we used 5 PC's to describe the augmented system. Concentration profiles of Mo-species calculated by MCR-ALS using augmented matrix are showed in Figure 10. Table 3 shows structural parameters obtained from EXAFS analysis and Figure 11 the XANES spectra. One observes that the precursor oxides from different Mo-loadings are quite similar. Minor differences between them were found on coordination number and bond distance for the first Mo-O contribution, as pointed out by EXAFS analysis: N = 1.8(4) and R = 1.73(1) Å compared to 3.5(6) and 1.746(5) in CoMo20. Further, the second Mo-O and Mo-Ti bonds present, respectively, an increased and a decreased bond length on CoMo5, 2.37(3) and 2.68(4) Å, compared to 1.96(1) and 2.73(3) Å on CoMo20. Such differences can be due to the way as the tiny CoMo5 particles interact with the support, maybe actually bound to it. Since Mo concentration is considerably smaller this interaction could be facilitated (instead of interaction with Co atoms, for instance, since no Mo-Co contribution was found). Our group reported that textural properties of the support may be changed in function of Mo concentration after calcination [22], [49] and that the support can impose the arrangement of the structure of the catalyst [50]. Then, effect of support on evolution of particle seems to be stronger in low loadings of precursors, as also found elsewhere [51], [52].

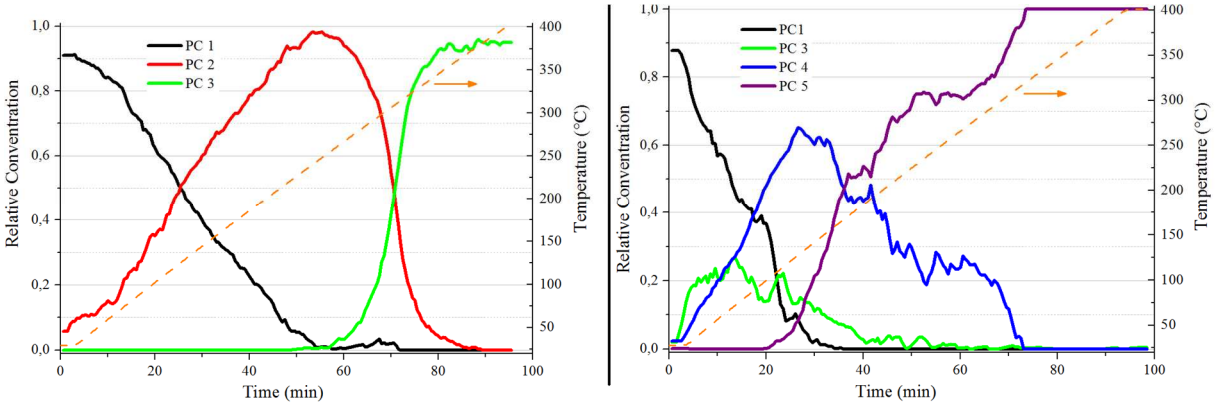

Figure 10 - MCR results for CoMo5 @ Mo K-edge, (left) concentration profiles of individual components during TPR and (right) during activation.

In TPR (Figure 10, left) structural analysis reveals that precursor oxide (PC1, black line) transforms in a second non-reduced oxide before to be completely reduced. Since this species starts to be formed as soon as reaction begins and reaches the maximum in higher temperatures (250 °C), it is probably a kind of dehydrated oxide and it will be called “heated oxide” (PC2, red). Actually, EXAFS results show that this component has basically the same bond distances than the precursor and an important change on coordination numbers. This component is more oxygen-coordinated and less Ti- and Mo-coordinated, which may indicate strong synergy (via oxygen exchange) between the catalyst and the support.

Reduced CoMo5 (PC3) starts to be formed in a lower temperature (250 °C) when compared to CoMo20 (320 °C), but they are relatively similar. Comparing both EXAFS results it seems that this component is a simplified version of that from CoMo20. In activation (Figure 10, right), important differences are observed when compared to high Mo-loading activation. Two intermediate species arise as soon the reaction begins, one of them a reduced oxide (green, the common species between TPR and activation) instead of a partially reduced oxide as in activation, whereas oxysulfide phase (PC4) is the other. It is noteworthy that besides the differences between the kinetics of the two reactions (CoMo20 and CoMo5), structurally

speaking, the evolution of the species from reduced to active phase is quite similar. For instance, the oxy-sulfide component for the CoMo5 has a Mo-O coordination number considerably larger and lower S-neighbors. Further, the shorter Mo-Mo on CoMo5 for this component indicates that the oxysulfide is closer to the reduced component than active phase. On CoMo20 we observe an inverse trend. However, the active phase is a MoS_2-like phase, as in CoMo20, but with no Mo-Co contribution.

Table 3 - Fitted Parameters at Mo K-edge (E_0 = 20004 ± 1 eV, S_0^2 = 0.96) and Co K-edge (E_0 = 7709 ± 1 eV, S_0^2 = 0.85)

Backscatterer	N	σ^2 (Å^2) x 10^{-3}	R (Å)
Mo K edge			
Precursor Oxide (PC 1)			
O	1.8 ± 0.4	3 ± 2	1.73 ± 0.01
O	1.8 ± 0.4	6 ± 4	2.37 ± 0.03
Ti	0.6 ± 0.2	6 ± 4	2.68 ± 0.04
Mo	1.0 ± 1.0	2 ± 9	3.24 ± 0.02
Mo	1.0 ± 1.0	2 ± 9	3.38 ± 0.03
ΔE = 0 eV, r-factor = 0.05, χ^2 = 621, N_{ind} = 14, N_{var} = 11			
Heated Oxide (PC 2)			
O	3.1 ± 0.5	8 ± 1	1.715 ± 0.005
O	2.6 ± 0.6	8 ± 1	2.37 ± 0.02
Ti	0.3 ± 0.1	6 ± 4	2.60 ± 0.06
Mo	0.6 ± 0.1	10 ± 4	3.25 ± 0.02
ΔE = 0 eV, r-factor = 0.009, χ^2 = 392, N_{ind} = 11, N_{var} = 9			
Reduced Oxide (PC 3)			
O	2.4 ± 0.9	1 ± 3	2.01 ± 0.01
Mo	0.3 ± 0.2	1 ± 3	2.62 ± 0.03
Mo	0.3 ± 0.2	1 ± 3	3.27 ± 0.06
ΔE = 3.2 eV, r-factor = 0.05, χ^2 = 240, N_{ind} = 8, N_{var} = 6			
Oxisulfide (PC 4)			
O	1.8 ± 0.5	4 ± 2	1.99 ± 0.008
S	0.5 ± 0.1	4 ± 2	2.34 ± 0.03
Mo	0.5 ± 0.1	4 ± 2	2.44 ± 0.01
ΔE = 5.5 eV, r-factor = 0.01, χ^2 = 196, N_{ind} = 7, N_{var} = 6			
Active Phase (PC 5)			
S	5.2 ± 0.3	5.2 ± 0.6	2.404 ± 0.005
Mo	3.0 ± 0.8	7 ± 1	3.167 ± 0.007
ΔE = 5.5 ± 0.8 eV, r-factor = 0.007, χ^2 = 115, N_{ind} = 14, N_{var} = 7			
Co K edge			
Precursor Oxide			
O	4.7 ± 1.1	7 ± 1	2.03 ± 0.01
Co	0.9 ± 0.4	8 ± 5	2.97 ± 0.03
Co	1.8 ± 1.0	8 ± 5	3.45 ± 0.02
ΔE = -1.7 ± 2.6 eV, r-factor = 0.0037, χ^2 = 7.14967, N_{ind} = 10, N_{var} = 9			

Finally, EXAFS analysis of precursor oxide at Co K-edge reveals a structure completely distinct when compared to the CoMo20 sample. One Co-O and two Co-Co contributions were quite suitable to fit experimental data, as displayed in Table 3. No Co-Mo distance reciprocal to the fit at Mo K-edge was found, which makes us wonder if in that case we are dealing with

separate Mo and Co phases, instead of single CoMo phase. XANES of sulfide Co-phase are compared in Figure S14. The main difference is the presence of a white-line in CoMo5, which indicates an incomplete sulfidation or even a segregation between Mo-species and Co-species in this catalyst. In other words, we cannot ensure the formation of a single CoMoS phase.

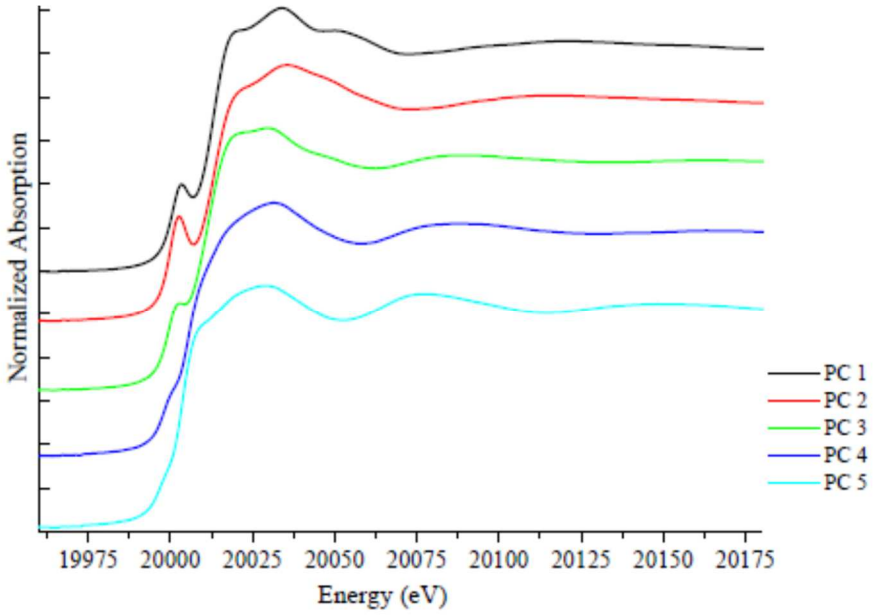

Figure 11 - MCR spectra of pure species obtained using augmented matrix for CoMo5 @ Mo K-edge.

It seems clear that CoMo5 is more sensitive to temperature and H_2S interaction and the simple thumb rule of same kinetic reaction for solids with different Mo concentration is not valid even if the same method was used for synthesis. Moreover, those findings suggest that concentration of precursor species may effectively play a structural role in the genesis of the active phase, which leads to different performances and efficiencies (probably mediated by the interaction with the support).

CONCLUSIONS

We have used chemometric tools to resolve the genesis of the active phase of the widely used CoMo-based HDS catalyst. This method was applied to time-resolved *in situ* XAS data. PCA

analysis was systematically used in order to evaluate the number of components of our matrix systems, namely, single activation matrix, single reduction matrix and gathered reduction-activation matrix. We have seen that step-by-step PCA analysis is a crucial procedure in order to better know the behavior of the system and to predict some features. The tools provided from PCA allied to a good previous knowledge of the system can give us a full description of a reaction by applying correctly MCR-ALS procedures.

With this method we have demonstrated that single matrix analysis of isolated reactions can give slightly, but important, different results in terms of kinetics and intermediate components of those actual transformations. For a high loading catalyst, the reduction matrix showed a issue for PC number determination though activation analysis gives right number of steps. It is just performing augmented analysis we could assign an intermediary step to TPR, and a reduced-like component formed on high temperature (~ 275 °C). Moreover, we could attribute correctly this species as a first intermediary step of activation. Interestingly, this component is formed at considerably lower temperature in this reaction (ca ~ 50 °C), which casts light on the role of H_2S as a reducing agent stronger than H_2 at low temperatures. We identified a 2nd intermediate as being an oxy-sulfide species, which turns to be transformed into the active CoMoS phase. Structurally, we were able to follow progressively the transformation of the precursor into the active phase. Further, evolution of Co species as found by MCR agrees (at least qualitatively) with recent XAS and RIXS experiments [51], suggesting single CoMoS phase formation but with a remaining Co-sulfide species.

Compared to a lower Mo-loading similar experiment, despite having a precursor with a molecular structure comparable to the corresponding catalyst with high Mo-loading, augmented analysis revealed a divergent kinetics during both TPR and activation. We found no partially reduced (or a first reduce-like species) catalyst on TPR, and direct transformation

of oxidic precursor into oxy-sulfide phase competing with the reduction. These findings suggest that not only the amount of precursor available to become the active phase plays a main role in catalytic efficiency, but also its quantity relative to the support, which will lead to contrasting evolution to active phase.

Summarily, MCR-ALS has been proving a powerful tool to be applied to time-resolved XAS experiments. We highlight that augmented-matrices approach offers new horizons in analysis and experiments designs, since it allows in one single package the analysis of combined and complementary techniques from a single experiment, as is progressively being done from some years mainly by Rochet/Briois group [19], [27], [29], [34], [44]. However, a careful planning of experiments takes a vital importance to obtain reliable results, avoiding rank deficient data and mistake in the assignment of the intermediates.

REFERENCES

[1] V. Chandra Srivastava, "An evaluation of desulfurization technologies for sulfur removal from liquid fuels," *RSC Advances*, vol. 2, no. 3, pp. 759–783, Jan. 2012, doi: 10.1039/C1RA00309G.

[2] A. Knop-Gericke *et al.*, "Chapter 4 X-Ray Photoelectron Spectroscopy for Investigation of Heterogeneous Catalytic Processes," *Advances in Catalysis*, vol. 52, no. C, pp. 213–272, Jan. 2009, doi: 10.1016/S0360-0564(08)00004-7.

[3] S. R. Bare and T. Ressler, "Chapter 6 Characterization of Catalysts in Reactive Atmospheres by X-ray Absorption Spectroscopy," *Advances in Catalysis*, vol. 52, no. C, pp. 339–465, Jan. 2009, doi: 10.1016/S0360-0564(08)00006-0.

[4] H. Topsøe, "Developments in operando studies and in situ characterization of heterogeneous catalysts," *Journal of Catalysis*, vol. 216, no. 1–2, pp. 155–164, May 2003, doi: 10.1016/S0021-9517(02)00133-1.

[5] D. D. Whitehurst, T. Isoda, and I. Mochida, "Present State of the Art and Future Challenges in the Hydrodesulfurization of Polyaromatic Sulfur Compounds," *Advances in Catalysis*, vol. 42, no. C, pp. 345–471, Jan. 1998, doi: 10.1016/S0360-0564(08)60631-8.

[6] H. Topsøe, B. S. Clausen, R. Candia, C. Wivel, and S. Mørup, “In situ Mössbauer emission spectroscopy studies of unsupported and supported sulfided Co□Mo hydrodesulfurization catalysts: Evidence for and nature of a Co□Mo□S phase,” *Journal of Catalysis*, vol. 68, no. 2, pp. 433–452, Apr. 1981, doi: 10.1016/0021-9517(81)90114-7.

[7] J. v. Lauritsen *et al.*, “Atomic-Scale Structure of Co–Mo–S Nanoclusters in Hydrotreating Catalysts,” *Journal of Catalysis*, vol. 197, no. 1, pp. 1–5, Jan. 2001, doi: 10.1006/JCAT.2000.3088.

[8] F. Besenbacher and J. v. Lauritsen, “Applications of high-resolution scanning probe microscopy in hydroprocessing catalysis studies,” *Journal of Catalysis*, vol. 403, pp. 4–15, Nov. 2021, doi: 10.1016/J.JCAT.2021.02.003.

[9] C. Márquez-Alvarez, I. Rodríguez-Ramos, A. Guerrero-Ruiz, G. L. Haller, and M. Fernández-García, “Selective reduction of NO(x) with propene under oxidative conditions: Nature of the active sites on copper-based catalysts,” *J Am Chem Soc*, vol. 119, no. 12, pp. 2905–2914, Mar. 1997, doi: 10.1021/JA961629Y/ASSET/IMAGES/MEDIUM/JA961629YE00007.GIF.

[10] S. R. Wasserman, P. G. Allen, K. Shuh, J. J. Bucher, and N. M. Edelstein, “EXAFS and principal component analysis: A new shell game,” *Journal of Synchrotron Radiation*, vol. 6, no. 3, pp. 284–286, May 1999, doi: 10.1107/S0909049599000965.

[11] Q. Wang, J. C. Hanson, and A. I. Frenkel, “Solving the structure of reaction intermediates by time-resolved synchrotron x-ray absorption spectroscopy,” *The Journal of Chemical Physics*, vol. 129, no. 23, p. 234502, Dec. 2008, doi: 10.1063/1.3040271.

[12] A. de Juan and R. Tauler, “Chemometrics applied to unravel multicomponent processes and mixtures: Revisiting latest trends in multivariate resolution,” *Analytica Chimica Acta*, vol. 500, no. 1–2, pp. 195–210, Dec. 2003, doi: 10.1016/S0003-2670(03)00724-4.

[13] M. Garrido, F. X. Rius, and M. S. Larrechi, “Multivariate curve resolution–alternating least squares (MCR-ALS) applied to spectroscopic data from monitoring chemical reactions processes,” *Analytical and Bioanalytical Chemistry 2008 390:8*, vol. 390, no. 8, pp. 2059–2066, Mar. 2008, doi: 10.1007/S00216-008-1955-6.

[14] A. de Juan, M. Maeder, M. Martínez, and R. Tauler, “Combining hard- and soft-modelling to solve kinetic problems,” *Chemometrics and Intelligent Laboratory Systems*, vol. 54, no. 2, pp. 123–141, Dec. 2000, doi: 10.1016/S0169-7439(00)00112-X.

[15] J. Hong *et al.*, “Speciation of ruthenium as a reduction promoter of silica-supported co catalysts: A time-resolved in situ XAS investigation,” *ACS Catalysis*, vol. 5, no. 2, pp. 1273–1282, Feb. 2015, doi: 10.1021/CS501799P/ASSET/IMAGES/LARGE/CS-2014-01799P_0008.JPEG.

[16] A. Voronov, A. Urakawa, W. van Beek, N. E. Tsakoumis, H. Emerich, and M. Rønning, “Multivariate curve resolution applied to in situ X-ray absorption spectroscopy data: An efficient tool for data processing and analysis,” *Analytica Chimica Acta*, vol. 840, pp. 20–27, Aug. 2014, doi: 10.1016/J.ACA.2014.06.050.

[17] W. H. Cassinelli *et al.*, “Multivariate curve resolution analysis applied to time-resolved synchrotron X-ray Absorption Spectroscopy monitoring of the activation of copper alumina

catalyst," *Catalysis Today*, vol. 229, pp. 114–122, Jun. 2014, doi: 10.1016/J.CATTOD.2013.10.077.

[18] P. Conti, S. Zamponi, M. Giorgetti, M. Berrettoni, and W. H. Smyrl, "Multivariate curve resolution analysis for interpretation of dynamic Cu k-edge X-ray absorption spectroscopy spectra for a Cu doped V2O 5 lithium battery," *Analytical Chemistry*, vol. 82, no. 9, pp. 3629–3635, May 2010, doi: 10.1021/AC902865H/SUPPL_FILE/AC902865H_SI_001.PDF.

[19] A. Rochet, B. Baubet, V. Moizan, C. Pichon, and V. Briois, "Co-K and Mo-K edges Quick-XAS study of the sulphidation properties of Mo/Al2O3 and CoMo/Al2O3 catalysts," *Comptes Rendus Chimie*, vol. 19, no. 10, pp. 1337–1351, Oct. 2016, doi: 10.1016/J.CRCI.2016.01.009.

[20] B. S. Clausen *et al.*, "Extended X-ray absorption fine structure study of Co-Mo hydrodesulfurization catalysts," *Journal of Physical Chemistry*, vol. 85, no. 25, pp. 3868–3872, 1981, doi: 10.1021/J150625A032/ASSET/J150625A032.FP.PNG_V03.

[21] J. Mazurelle, C. Lamonier, C. Lancelot, E. Payen, C. Pichon, and D. Guillaume, "Use of the cobalt salt of the heteropolyanion [Co2Mo10O38H4]6− for the preparation of CoMo HDS catalysts supported on Al2O3, TiO2 and ZrO2," *Catalysis Today*, vol. 130, no. 1, pp. 41–49, Jan. 2008, doi: 10.1016/J.CATTOD.2007.07.008.

[22] D. L. Nguyen *et al.*, "One-Pot Sol–Gel Preparation for Efficient Cobalt–Molybdenum–Titania Hydrotreating Catalysts," *ChemCatChem*, vol. 4, no. 12, pp. 2112–2120, Dec. 2012, doi: 10.1002/CCTC.201200165.

[23] N. Frizi *et al.*, "Genesis of new gas oil HDS catalysts: Study of their liquid phase sulfidation," *Catalysis Today*, vol. 130, no. 1, pp. 32–40, Jan. 2008, doi: 10.1016/J.CATTOD.2007.10.008.

[24] F. P. J. M. Kerkhof and J. A. Moulijn, "Quantitative analysis of XPS intensities for supported catalysts," *Journal of Physical Chemistry*, vol. 83, no. 12, pp. 1612–1619, 1979, doi: 10.1021/J100475A011/ASSET/J100475A011.FP.PNG_V03.

[25] E. Fonda, A. Rochet, M. Ribbens, L. Barthe, S. Belin, and V. Briois, "The SAMBA quick-EXAFS monochromator: XAS with edge jumping," *Journal of Synchrotron Radiation*, vol. 19, no. 3, pp. 417–424, May 2012, doi: 10.1107/S0909049512009703/IE5068SUP1.PDF.

[26] V. Briois *et al.*, "SAMBA: The 4–40 keV X-ray absorption spectroscopy beamline at SOLEIL," in *UVX 2010 - 10e Colloque sur les Sources Cohérentes et Incohérentes UV, VUV et X ; Applications et Développements Récents*, Mar. 2011, pp. 41–47. doi: 10.1051/uvx/2011006.

[27] A. Rochet, V. Moizan, F. Diehl, C. Pichon, and V. Briois, "Quick-XAS and Raman operando characterisation of a cobalt alumina-supported catalyst under realistic Fischer–Tropsch reaction conditions," *Catalysis Today*, vol. 205, pp. 94–100, Apr. 2013, doi: 10.1016/J.CATTOD.2012.08.021.

[28] C. la Fontaine, L. Barthe, A. Rochet, and V. Briois, "X-ray absorption spectroscopy and heterogeneous catalysis: Performances at the SOLEIL's SAMBA beamline," *Catalysis Today*, vol. 205, pp. 148–158, Apr. 2013, doi: 10.1016/J.CATTOD.2012.09.032.

[29] A. Rochet, V. Moizan, C. Pichon, F. Diehl, A. Berliet, and V. Briois, "In situ and operando structural characterisation of a Fischer–Tropsch supported cobalt catalyst," *Catalysis Today*, vol. 171, no. 1, pp. 186–191, Aug. 2011, doi: 10.1016/J.CATTOD.2011.03.079.

[30] B. Ravel and M. Newville, “ATHENA, ARTEMIS, HEPHAESTUS : data analysis for X-ray absorption spectroscopy using IFEFFIT,” *Journal of Synchrotron Radiation*, vol. 12, no. 4, pp. 537–541, Jul. 2005, doi: 10.1107/S0909049505012719.

[31] R. Tauler, “Multivariate curve resolution applied to second order data,” *Chemometrics and Intelligent Laboratory Systems*, vol. 30, no. 1, pp. 133–146, Nov. 1995, doi: 10.1016/0169-7439(95)00047-X.

[32] A. Martini and E. Borfecchia, “Spectral Decomposition of X-ray Absorption Spectroscopy Datasets: Methods and Applications,” *Crystals (Basel)*, vol. 10, no. 8, p. 664, Aug. 2020, doi: 10.3390/cryst10080664.

[33] A. Ribeiro Passos, C. la Fontaine, A. Rochet, and V. Briois, “Time-Resolved XAS applied to Heterogeneous Catalysis: Science Case,” in *Springer Handbook of Advanced Catalyst Characterization*, vol. In Press, I. Wachs and M. A. Bañares, Eds. Springer Chem, 2023.

[34] M. Nikulshina *et al.*, “Genesis of active phase in MoW/Al2O3 hydrotreating catalysts monitored by HAADF and in situ QEXAFS combined to MCR-ALS analysis,” *Applied Catalysis B: Environmental*, vol. 269, p. 118766, Jul. 2020, doi: 10.1016/J.APCATB.2020.118766.

[35] J. Jaumot, A. de Juan, and R. Tauler, “MCR-ALS GUI 2.0: New features and applications,” *Chemometrics and Intelligent Laboratory Systems*, vol. 140, pp. 1–12, Jan. 2015, doi: 10.1016/J.CHEMOLAB.2014.10.003.

[36] S. Kasztelan, J. Grimblot, J. P. Bonnelle, E. Payen, H. Toulhoat, and Y. Jacquin, “Preparation of Co-Mo-γAl2O3 and Ni-Mo-γAl2O3 catalysts by ph regulation of molybdenum solution. characterization of supported species and hydrogenation activities,” *Applied Catalysis*, vol. 7, no. 1, pp. 91–112, Jul. 1983, doi: 10.1016/0166-9834(83)80241-3.

[37] P. R. Peres-Neto, D. A. Jackson, and K. M. Somers, “How many principal components? stopping rules for determining the number of non-trivial axes revisited,” *Computational Statistics & Data Analysis*, vol. 49, no. 4, pp. 974–997, Jun. 2005, doi: 10.1016/J.CSDA.2004.06.015.

[38] J. Stoer and R. Bulirsch, *Introduction to Numerical Analysis*. New York, NY: Springer New York, 2002. doi: 10.1007/978-0-387-21738-3.

[39] M. J. Fay, A. Proctor, D. P. Hoffmann, M. Houalla, and D. M. Hercules, “Determination of the Mo surface environment of Mo/TiO2 catalysts by EXAFS, XANES and PCA,” *Microchimica Acta 1992 109:5*, vol. 109, no. 5, pp. 281–293, Sep. 1992, doi: 10.1007/BF01242483.

[40] S. R. Wasserman, “The Analysis of Mixtures: Application of Principal Component Analysis to XAS Spectra,” *Le Journal de Physique IV*, vol. 7, no. C2, pp. C2-203-C2-205, Apr. 1997, doi: 10.1051/jp4/1997163.

[41] R. M. M. Santos, V. Briois, L. Martins, and C. v. Santilli, “Insights into the Preparation of Copper Catalysts Supported on Layered Double Hydroxide Derived Mixed Oxides for Ethanol Dehydrogenation,” *ACS Applied Materials and Interfaces*, vol. 13, no. 22, pp. 26001–26012, Jun. 2021, doi: 10.1021/ACSAMI.1C04541/ASSET/IMAGES/LARGE/AM1C04541_0010.JPEG.

[42] R. G. Leliveld, A. J. van Dillen, J. W. Geus, and D. C. Koningsberger, “A Mo–K Edge XAFS Study of the Metal Sulfide-Support Interaction in (Co)Mo Supported Alumina and Titania Catalysts,” *Journal of Catalysis*, vol. 165, no. 2, pp. 184–196, Jan. 1997, doi: 10.1006/JCAT.1997.1480.

[43] T. Weber, J. C. Muijsers, J. H. M. C. van Wolput, C. P. J. Verhagen, and J. W. Niemantsverdriet, "Basic reaction steps in the sulfidation of crystalline MoO3 to MoS2, as studied by X-ray photoelectron and infrared emission spectroscopy," *Journal of Physical Chemistry*, vol. 100, no. 33, pp. 14144–14150, Aug. 1996, doi: 10.1021/JP961204Y/ASSET/IMAGES/LARGE/JP961204YFB56E.JPEG.

[44] A. Rochet *et al.*, "Intermediate Species Revealed during Sulfidation of Bimetallic Hydrotreating Catalyst: A Multivariate Analysis of Combined Time-Resolved Spectroscopies," *Journal of Physical Chemistry C*, vol. 121, no. 34, pp. 18544–18556, Aug. 2017, doi: 10.1021/ACS.JPCC.7B03735/ASSET/IMAGES/LARGE/JP-2017-03735G_0008.JPEG.

[45] P. Afanasiev *et al.*, "Low-Temperature Hydrogen Interaction with Amorphous Molybdenum Sulfides MoSx," *Journal of Physical Chemistry C*, vol. 113, no. 10, pp. 4139–4146, Mar. 2009, doi: 10.1021/JP809300Y.

[46] S. AN, "The Reaction Mechanisms of H2S Decomposition into Hydrogen and Sulfur: Application of Classical and Biological Thermodynamics," *Journal of Thermodynamics & Catalysis*, vol. 08, no. 02, 2017, doi: 10.4172/2157-7544.1000186.

[47] L. Plais, C. Lancelot, C. Lamonier, E. Payen, and V. Briois, "First in situ temperature quantification of CoMoS species upon gas sulfidation enabled by new insight on cobalt sulfide formation," *Catalysis Today*, vol. 377, pp. 114–126, Oct. 2021, doi: 10.1016/J.CATTOD.2020.06.065.

[48] A. Tougerti *et al.*, "Rethinking Electronic and Geometric Structures of Real Hydrodesulfurization Catalysts by in Situ Photon-In/Photon-Out Spectroscopy," *Journal of Physical Chemistry C*, vol. 124, no. 32, pp. 17586–17598, Aug. 2020, doi: 10.1021/ACS.JPCC.0C03429/SUPPL_FILE/JP0C03429_SI_001.PDF.

[49] C. la Fontaine *et al.*, "Methanol conversion over TiO2-anatase supported oxomolybdate catalysts: an integrated operando – DFT modeling approach," *https://doi.org/10.1080/01411594.2011.578825*, vol. 84, no. 8, pp. 700–713, Aug. 2011, doi: 10.1080/01411594.2011.578825.

[50] A. Tougerti *et al.*, "Synergy between XANES Spectroscopy and DFT to Elucidate the Amorphous Structure of Heterogeneous Catalysts: TiO2-Supported Molybdenum Oxide Catalysts," *Angewandte Chemie International Edition*, vol. 52, no. 25, pp. 6440–6444, Jun. 2013, doi: 10.1002/ANIE.201300538.

[51] C. Andriopoulou and S. Boghosian, "Tuning the configuration of dispersed oxometallic sites in supported transition metal oxide catalysts: A temperature dependent Raman study," *Catalysis Today*, vol. 336, pp. 74–83, Oct. 2019, doi: 10.1016/J.CATTOD.2019.01.080.

[52] G. Tsilomelekis *et al.*, "Molybdena deposited on titania by equilibrium deposition filtration: structural evolution of oxo–molybdenum(VI) sites with temperature," *Physical Chemistry Chemical Physics*, vol. 18, no. 34, pp. 23980–23989, Aug. 2016, doi: 10.1039/C6CP05247A.